

An orifice shape-based reduced order model of patient-specific mitral valve regurgitation

J. Franz, K. Czechowicz, I. Waechter-Stehle, F. Hellmeier, F. Razafindrazaka, M. Kelm, J. Kempfert, A. Meyer, G. Archer, J. Weese, R. Hose, T. Kuehne & L. Goubergrits

To cite this article: J. Franz, K. Czechowicz, I. Waechter-Stehle, F. Hellmeier, F. Razafindrazaka, M. Kelm, J. Kempfert, A. Meyer, G. Archer, J. Weese, R. Hose, T. Kuehne & L. Goubergrits (2021) An orifice shape-based reduced order model of patient-specific mitral valve regurgitation, *Engineering Applications of Computational Fluid Mechanics*, 15:1, 1868-1884, DOI: [10.1080/19942060.2021.1995048](https://doi.org/10.1080/19942060.2021.1995048)

To link to this article: <https://doi.org/10.1080/19942060.2021.1995048>



© 2021 The Author(s). Published by Informa UK Limited, trading as Taylor & Francis Group



[View supplementary material](#)



Published online: 23 Nov 2021.



[Submit your article to this journal](#)



Article views: 750



[View related articles](#)



[View Crossmark data](#)

An orifice shape-based reduced order model of patient-specific mitral valve regurgitation

J. Franz^a, K. Czechowicz^b, I. Waechter-Stehle^c, F. Hellmeier^a, F. Razafindrazaka^a, M. Kelm^{a,d,e}, J. Kempfert^{e,f}, A. Meyer^{e,f}, G. Archer^g, J. Weese^c, R. Hose^b, T. Kuehne^{a,d,e} and L. Goubergrits^{a,h}

^aInstitute of Computer-assisted Cardiovascular Medicine, Charité – Universitätsmedizin Berlin, Berlin, Germany; ^bDepartment of Infection, Immunity and Cardiovascular Disease, The University of Sheffield, Sheffield, UK; ^cPhilips Research, Hamburg, Germany; ^dDepartment of Congenital Heart Disease, German Heart Center Berlin (DHZB), Berlin, Germany; ^ePartner Site Berlin, German Center for Cardiovascular Research (DZHK), Berlin, Germany; ^fDepartment of Cardiothoracic and Vascular Surgery, German Heart Center Berlin (DHZB), Berlin, Germany; ^gCardiothoracic Centre, Sheffield Teaching Hospital NHS Foundation Trust, Sheffield, UK; ^hEinstein Center Digital Future (ECDF), Berlin, Germany

ABSTRACT

Mitral valve regurgitation (MR) is one of the most prevalent valvular heart diseases. Its quantitative assessment is challenging but crucial for treatment decisions. Using computational fluid dynamics (CFD), we developed a reduced order model (ROM) describing the relationship between MR flow rates, transvalvular pressure differences, and the size and shape of the regurgitant valve orifice. Due to its low computational cost, this ROM could easily be implemented into clinical workflows to support the assessment of MR. We reconstructed mitral valves of 43 patients from 3D transesophageal echocardiographic images and estimated the 3D anatomic regurgitant orifice areas using a shrink-wrap algorithm. The orifice shapes were quantified with three dimensionless shape parameters. Steady-state CFD simulations in the reconstructed mitral valves were performed to analyse the relationship between the regurgitant orifice geometry and the regurgitant hemodynamics. Based on the results, three ROMs with increasing complexity were defined, all of which revealed very good agreement with CFD results with a mean bias below 3% for the MR flow rate. Classifying orifices into two shape groups and assigning group-specific flow coefficients in the ROM reduced the limit of agreement predicting regurgitant volumes from 9.0 ml to 5.7 ml at a mean regurgitant volume of 57 ml.

ARTICLE HISTORY

Received 14 May 2021
Accepted 13 October 2021

KEYWORDS

Mitral valve regurgitation; pressure gradient; computational fluid dynamics; regurgitant orifice area; 3D transesophageal echocardiography; patient-specific model

1. Introduction


Mitral valve regurgitation (MR) is one of the most prevalent valvular heart diseases (Iung et al., 2007; Nkomo et al., 2006). It is characterized by the inability of the mitral valve to close properly during the heart's ejection phase (systole), leading to an abnormal backflow of blood from the left ventricle into the left atrium. A distinction is made between primary MR caused by abnormalities at the valve apparatus itself, and secondary MR, which results from pathological changes of the left ventricular geometry. Severe MR can lead to pulmonary hypertension, atrial fibrillation and heart failure, and often requires treatment in form of valve repair or replacement. Echocardiography serves as the standard clinical tool to assess MR and both qualitative and quantitative parameters contribute to the grading of MR severity (El-Tallawi et al., 2017; Zoghbi et al., 2017). However, due to the complexity of the disease and the multitude of underlying

causes, choosing the optimal treatment and the timing of intervention remains challenging (Baumgartner et al., 2017; Nishimura et al., 2017).

To support the diagnosis and treatment decisions for patients with MR, computational models of cardiovascular hemodynamics may serve as a useful tool. Computational fluid dynamics (CFD) models can provide detailed 3D insights into local blood flow phenomena at various cardiovascular sites (Doost et al., 2016; Kang et al., 2021; Mittal et al., 2016; Sun et al., 2019), including the (diseased) mitral valve (This et al., 2020; Vellguth et al., 2018, 2019; Votta et al., 2013). However, since the application of CFD models is time consuming and computationally expensive, their implementation into fast-paced clinical workflows is often not feasible. Therefore, fast and computationally inexpensive reduced-order and lumped parameter models, which can simulate relevant aspects of a patient's hemodynamic state under various

CONTACT J. Franz  juliana.franz@charite.de

Trial registration: ClinicalTrials.gov identifier: NCT04068740.

 Supplemental data for this article can be accessed here. <https://doi.org/10.1080/19942060.2021.1995048>

© 2021 The Author(s). Published by Informa UK Limited, trading as Taylor & Francis Group
This is an Open Access article distributed under the terms of the Creative Commons Attribution-NonCommercial License (<http://creativecommons.org/licenses/by-nc/4.0/>), which permits unrestricted non-commercial use, distribution, and reproduction in any medium, provided the original work is properly cited.

conditions, are a promising alternative to 3D models in clinical practice (Bubak et al., 2021; Huttary et al., 2017; Meiburg et al., 2020; Mynard et al., 2012; Paeme et al., 2010; Shi et al., 2011).

The aim of our study is to develop a reduced order model of MR describing the relationship between the regurgitant blood flow rate, the blood pressure difference across the mitral valve and the geometry of the regurgitant valve orifice, which could be implemented in clinical practice to support the quantitative assessment of MR. Since an accurate, simultaneous assessment of regurgitant blood flow, blood pressure and the regurgitant valve shape is difficult to impossible to achieve in-vivo, we use CFD models to simulate the regurgitant blood flow in echocardiography-based 3D reconstructions of patient-specific mitral valves. The simulation results then serve as the basis for the reduced order model development.

By assuming an incompressible, quasi-steady flow, the regurgitant blood flow through the mitral valve in a reduced order model may be modeled based on Bernoulli's principle and continuity of flow as

$$Q = c_D \cdot AROA \cdot \sqrt{\frac{2\Delta p}{\rho}} \quad (1)$$

with Q the volumetric flow rate, Δp the transvalvular pressure difference (in clinical practice commonly referred to as transvalvular pressure gradient), ρ the blood density, $AROA$ the anatomic regurgitant orifice area and c_D the dimensionless discharge coefficient. In a clinical context, with commonly used units of blood flow rate in ml/s, orifice area in cm^2 , blood pressure in mmHg (1 mmHg \approx 133.3 Pa), and a density of blood of $\rho = 1060 \text{ kg/m}^3$, (1) can be written as

$$Q = c \cdot AROA \cdot \sqrt{\Delta p} \quad (2)$$

with a dimensional flow coefficient c defined as

$$c = 50.2 \cdot c_D \frac{\text{cm}}{\text{s}\sqrt{\text{mmHg}}} \quad (3)$$

In order to apply (2) to describe the patient-specific blood flow through regurgitant mitral valves, two main points need to be addressed, which are the focus of this study: (i) establishing a value or function describing the flow coefficient c for regurgitant mitral valve flow and (ii) developing a method to accurately assess the AROA in 3D space based on 3D echocardiographic images.

In general, the discharge coefficient c_D describes the ratio of the actual flow rate to the theoretical flow rate without irreversible losses and it can differ depending on orifice shape (e.g. degree of restriction, edge sharpness and orifice eccentricity) and flow state (i.e. laminar or turbulent) (Abd et al., 2019; Athar et al., 2003; Hollingshead et al., 2011). In the context of heart valves, flow

coefficients have been mainly investigated for stenotic mitral and aortic valves, which are characterized by a restrictive opening area and impaired leaflet motion. Empirically found values are $c = 37.9 \text{ cm/s}/\sqrt{\text{mmHg}}$ for stenotic mitral valves and $c = 44.3 \text{ cm/s}/\sqrt{\text{mmHg}}$ for stenotic aortic valves (Cohen & Gorlin, 1972; Gorlin & Gorlin, 1951). While it is difficult to study the influence of the valve shape on the flow coefficient in-vivo, experimental in-vitro studies have shown that orifice eccentricity and leaflet shape influence the flow coefficients through (idealized) stenotic mitral and aortic valve geometries (Flachskampf et al., 1990; Gilon et al., 2002). Regurgitant mitral valves show a variety of different morphologies, ranging from more circular to very elongated orifices, including complex 3D shapes with prolapsed or flail leaflets (Buchner et al., 2011). Flow coefficients of regurgitant mitral valve flow can thus be expected to vary depending on the orifice shape, but this has, to our knowledge, not been investigated to date.

The complex, non-circular and non-planar shape of the regurgitant mitral valve orifices also poses difficulties for the estimation of the AROA in 3D space. Clinical guidelines recommend two echocardiography-based methods to estimate the regurgitant orifice area: an indirect measurement of the effective regurgitant orifice area (EROA) using the proximal isovelocity surface area (PISA) method, and the 'en face' vena contracta area (VCA) using 3D Color Doppler imaging (El-Tallawi et al., 2017). However, both EROA and VCA estimations do not capture the full 3D nature of the regurgitant orifice. In patients with non-circular orifices, overlapping leaflets, multiple orifices or eccentric jets, these methods can be unreliable and highly observer-dependent (Biner et al., 2010; Coisne et al., 2020; Yosefy et al., 2009). For this reason, iterative methods to estimate the 'true' AROA in 3D space have been proposed (Chandra et al., 2011; Sotaquirá et al., 2017). AROA measurements by Chandra et al. (2011) deviated from EROA estimations in particular for patients with more complex orifice shapes and eccentric jets, for which EROA measurements are often unreliable. Sotaquirá et al. (2017) found significant levels of elongation and curvature in the shape of the majority of 25 investigated regurgitant orifices, highlighting the importance of considering the full 3D shape of the regurgitant orifice for an accurate representation.

In this study, we aim to develop a reduced order model to describe the patient-specific pressure gradient-flow rate relationship of regurgitant mitral valves using only geometrical information about the regurgitant orifice size and shape as patient-specific input. To estimate the patient-specific AROA, we provide a semi-automatic method to approximate the non-planar anatomic regurgitant orifice from transesophageal echocardiography (TEE)-based segmentations of the regurgitant mitral

valve. Using CFD, the regurgitant blood flow through the mitral valves of 43 patients with MR is simulated. The results of the CFD simulations and the regurgitant orifice estimations are used to investigate the regurgitant flow coefficients and their relationship with the orifice shape. Finally, three reduced order models of increasing complexity are defined to simulate the patient-specific MR, and their predictions are compared to the CFD results.

2. Methods

2.1. Study design

Figure 1 presents an overview of the methods used to investigate the flow coefficients of regurgitant mitral valves and the influence of the orifice shape. Segmented geometries of the mitral valve during regurgitation (A) were used to analyse the geometrical features of the regurgitant orifice (B + D) and to determine the regurgitant

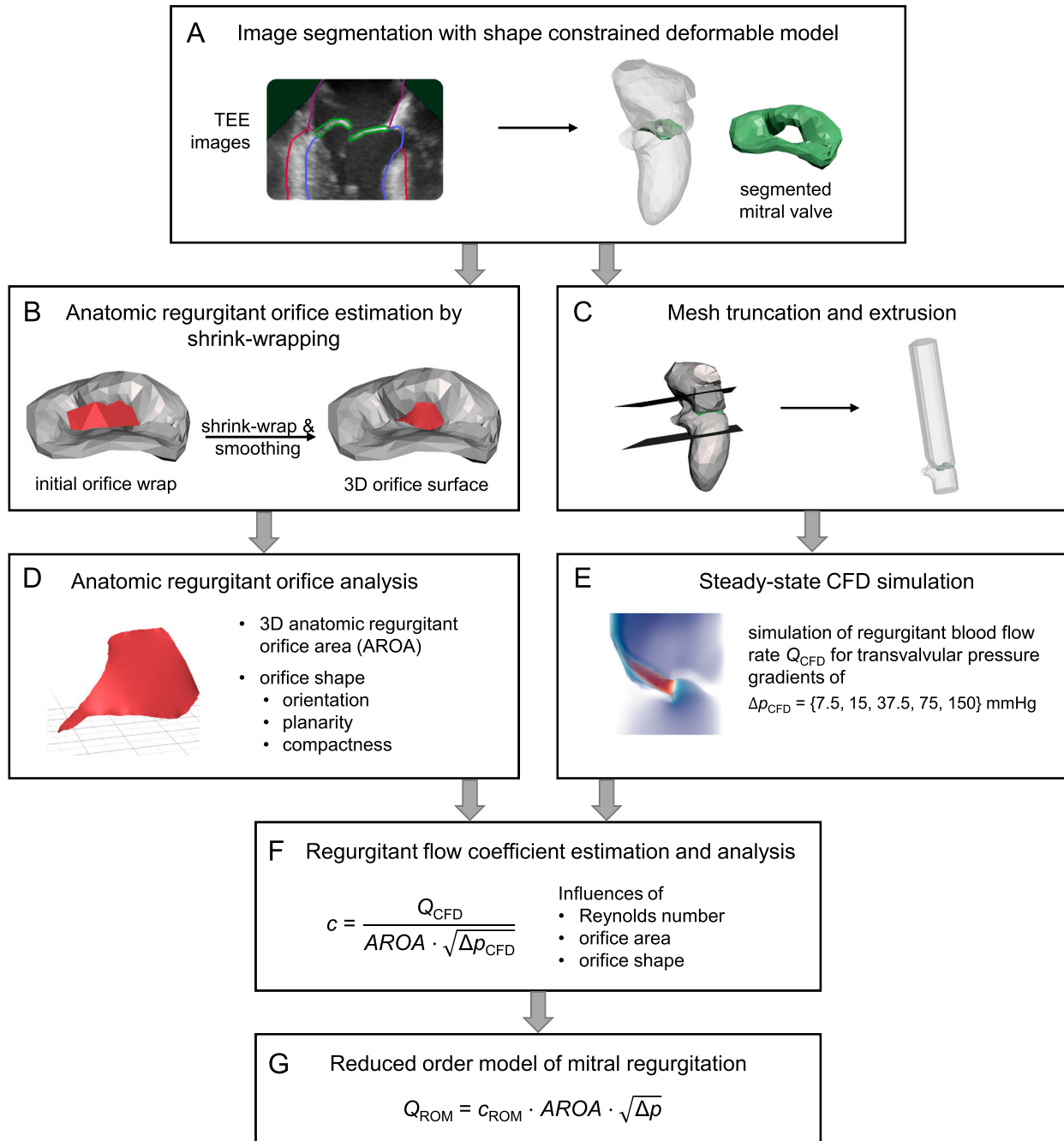


Figure 1. Methods overview for the estimation of flow coefficients in regurgitant mitral valves using approximations of the AROA and steady-state CFD simulations of blood flow through the regurgitant orifice. The resulting flow coefficients were analysed and used to develop reduced order models of different complexity to describe the patient-specific regurgitant mitral valve flow rate.

blood flow at different transvalvular pressure gradients using steady-state CFD simulations (C + E). The regurgitant flow coefficients were estimated using the results of the AROA estimations and the CFD simulated pressures and flow rates (F). Subsequently, the influence of the orifice shape on the flow coefficient was studied and the reduced order models were defined (G). In the following, the methods are described in detail.

2.2. Mitral valve segmentation

In this study, time-dependent 3D TEE sequences of the mitral valves of 43 MR patients (age 63 ± 11 years, 29 male) were used, which were acquired prior to the patients' surgical MR treatment. The majority of the patients had primary MR, with mitral valve prolapse being the most common cause (38 primary MR cases, of which 34 with prolapse). The datasets were obtained at two clinical centers: 25 cases from the German Heart Center Berlin and 18 cases from Sheffield Teaching Hospitals. Written informed consent was obtained from all patients and the procedures were approved by the local Ethical Committees (Ethikkommission Charité – Universitätsmedizin Berlin: EA2/093/16, NHS Health Research Authority: 17/LO/0283). The study is registered on ClinicalTrials.gov (NCT04068740). The TEE sequences were acquired with two ultrasound machines: GE Vivid E9 (General Electric, USA) at the German Heart Center Berlin and Philips iE33 (Philips, The Netherlands) at Sheffield Teaching Hospitals. From the time-dependent 3D TEE dataset of each patient, the 3D image at the time of most pronounced regurgitation was identified upon visual inspection. In these selected 3D TEE images, the regurgitant mitral valves as well as left atrium and left ventricle were segmented semi-automatically using a shape-constrained deformable model (Weber et al., 2015), as illustrated in Figure 1A.

2.3. Anatomic regurgitant orifice approximation

The anatomic regurgitant orifice surfaces of the segmented mitral valves were approximated using a

controlled shrink-wrap algorithm following Razafindrakaza et al. (2019). The process is illustrated in Figure 2. The mitral valve geometry served as the target surface T . An initial triangulated surface S was defined manually as a first approximation of the valve orifice and subsequently adaptively wrapped around T until no more movement was possible. In this iterative process, the displacement of nodes of S is aimed to minimize the Hausdorff distance between S and T (Razafindrakaza et al., 2019). Additional smoothing controls the elastic behavior of S during the shrink-wrap process. The final approximation of the orifice, $S_{orifice}$, was obtained as the part of S which does not cover T . The boundary faces of $S_{orifice}$ are close to orthogonal to T , which is desired to achieve a good approximation of the orifice area. The edge length of the triangles in S was manually adjusted during the shrink-wrap process to obtain optimal results.

The shrink-wrapped orifice surfaces were further processed by smoothing both surfaces and boundaries while ensuring that the surfaces continued to cover the entire valve orifice. Small corrections to the orifice surface were added in locations with very narrow openings. We tested the robustness of the orifice estimation method for two cases with significantly different orifice shapes, as shown in Figure 3 (one rather round with prolapsed leaflet and one more elongated). For both cases, two different initial wrapping surfaces were defined, and the subsequent steps (shrink wrapping and manual smoothing/correction) were performed two times by the same user for each result of the previous step. The coefficient of variation for the approximated orifice areas was below 2% in both cases.

2.4. Regurgitant orifice shape analysis

We characterized the orifices' shapes in 3D space with three dimensionless parameters describing their orientation, planarity and compactness, respectively. The orientation index aims to separate prolapsed and non-prolapsed mitral valve configurations during the regurgitation phase. Non-prolapsed configurations usually result in free jet flow, whereas prolapsed configurations usually lead to a wall jet. The planarity index is proposed

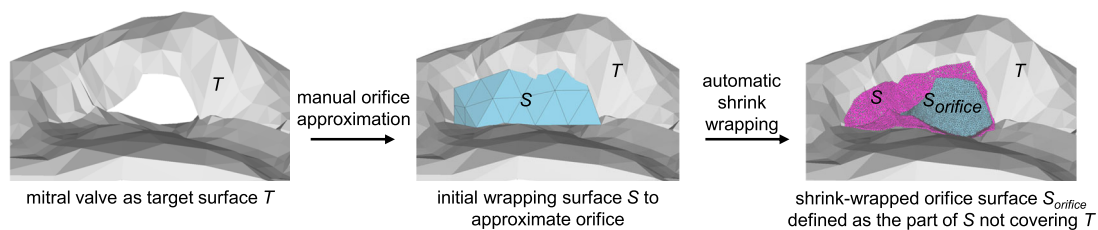


Figure 2. Shrink-wrap-based approximation of the anatomic regurgitant mitral valve orifice in 3D space.

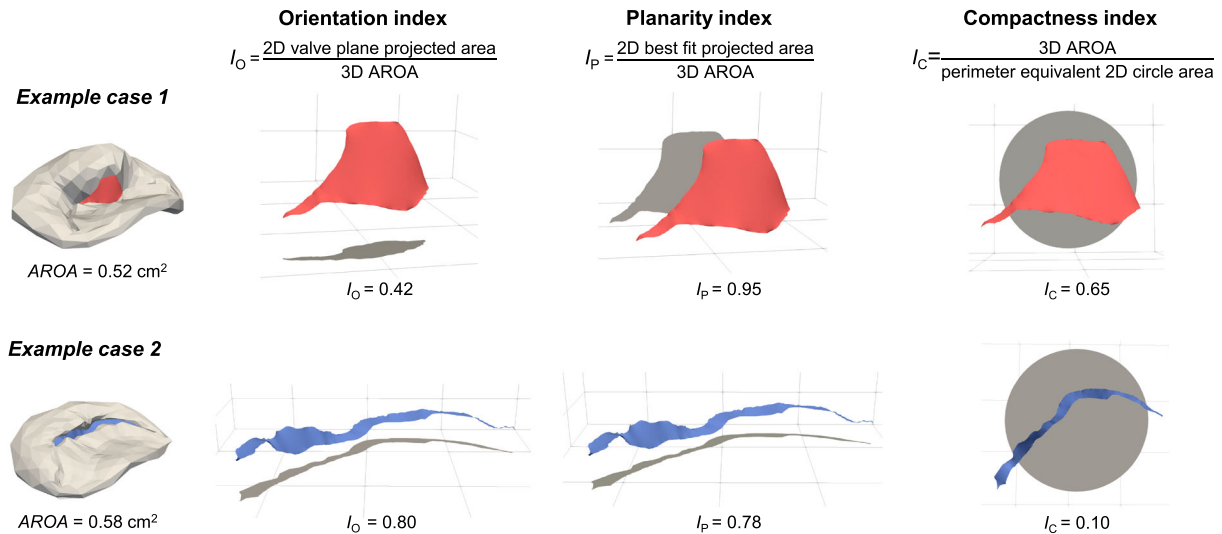


Figure 3. Definition of the three dimensionless shape parameters (orientation, planarity and compactness indices) to characterize the regurgitant mitral valve orifices in 3D space. The 2D (projected) areas used in the computation of the shape indices as well as the resulting index values are depicted for two example cases.

to describe the 3D shape complexity of the orifice. The compactness index describes the aspect ratio of the orifice, allowing to distinguish between more flat and more circular jets. Each of the three shape parameters is defined by an area ratio as illustrated in Figure 3 and as described in the following.

For the definition of the orientation and planarity indices, we approximated 2D projections of the 3D orifice surfaces onto two different planes: (i) the best-fitting valve plane with respect to the whole mitral valve geometry, and (ii) the best-fitting orifice plane, on which the projected orifice area was maximized. To determine these two best-fitting planes, we first computed the covariance matrix of the 3D point cloud defining (i) the mitral valve geometry and (ii) the 3D orifice surface, respectively. Using principal component analysis, the covariance matrix was decomposed into its eigenvectors and eigenvalues. The normal vector n of the best-fitting plane was determined as the cross product of the two eigenvectors that resulted in the maximum area projected onto a plane normal to n . The 2D projected areas of the 3D orifices onto the best-fitting planes were then approximated by alpha shapes with a manually adjusted alpha radius for each orifice.

The orientation index, I_O , is defined as the ratio between the valve-plane projected orifice area and the AROA. It describes the orientation of the orifice relative to the valve plane with values between 0 (perpendicular to the valve plane) to 1 (parallel to the valve plane). The planarity index, I_P , is defined as the ratio between the best-fitting projected orifice area and the AROA. It takes a value of 1 for planar orifices and its value decreases the more curved the orifice shape. The compactness index,

I_C , is defined as the ratio of the AROA and the area of a 2D circle with the same perimeter as the 3D orifice. A compactness of 1 denotes a circular orifice and the more elongated the orifice, the smaller the compactness. In cases with multiple orifices, the overall compactness index was computed as the orifice area-weighted sum of the compactness indices of the individual orifices.

2.5. Hemodynamic simulation

The segmented geometries of the regurgitant mitral valve, left atrium and left ventricle were truncated 2–3 cm above and below the mitral valve plane (cf. Figure 1C), as our main interest was the investigation of flow through the mitral valve itself. Both inlet (ventricular side) and outlet (atrial side) boundaries were extruded by straight pipes with a length of 2 cm and 20 cm, respectively, with the latter corresponding to about five times the mitral annulus diameter. Volumetric meshes were built in Ansys Fluent 19.0 (ANSYS Inc., USA) and were composed of tetrahedra in the core and five inflation layers with prism-shaped cells at the wall. The mesh, which was elaborated after a mesh independence study, contains elements with edge lengths ranging from 0.1 mm near the valve to around 3.5 mm in the extrusion pipes. We simulated blood flow through the regurgitant mitral valves at a single time point during mid-systole, at which the regurgitation was most pronounced. Blood was modeled as an incompressible Newtonian fluid with a density of $\rho = 1060 \text{ kg}\cdot\text{m}^{-3}$ (Hinghofer-Szalkay et al., 1979) and a dynamic viscosity of $\eta = 0.004 \text{ Pa}\cdot\text{s}$ (Rosenson et al., 1996). Although in general, blood is a shear-thinning fluid, it can be considered Newtonian at higher shear

rates $>100/s$ (Cherry & Eaton, 2013), which are expected in the regurgitant jets. The continuity and momentum equations describing incompressible fluid flow are given by

$$\nabla \mathbf{u} = 0 \quad (4)$$

$$\rho \left(\frac{\partial \mathbf{u}}{\partial t} + (\mathbf{u} \cdot \nabla) \mathbf{u} \right) = -\nabla p + \eta \Delta \mathbf{u} + \mathbf{f} \quad (5)$$

with velocity vector \mathbf{u} , pressure p and external forces \mathbf{f} . They were solved numerically with Ansys Fluent 19.0 for the steady state ($\partial \mathbf{u} / \partial t = 0$). Turbulence was modeled with the two-equation shear stress transport (SST) k-omega model, which performs well in both near-wall and freestream regions (Aftab et al., 2016). Since our study is not focused on analysing fine-grained turbulent fluctuations, a two-equation model is considered sufficient for the purpose of quantifying the regurgitant flow rate across a leaking valve. This is in agreement with other simulation studies, who have demonstrated that clinically relevant hemodynamic parameters such as the pressure drop over a stenosis or the regurgitant volume caused by paravalvular leakage are independent of turbulent parameters (Bianchi et al., 2019; Itu et al., 2013). The pressure at the outlet boundary was set to zero for all simulations and no-slip boundary conditions were assumed at the walls. For each mitral valve, five steady flow simulations with different inlet pressure boundary conditions ranging from 1 kPa to 20 kPa (7.5–150 mmHg) were performed, covering a typical range of transvalvular pressure gradients during systole. The simulated flow rates were assessed at the inlet boundary and are provided for all

cases and simulations as supplemental data to this study. Figure 4 shows the simulated regurgitant jets for two example cases.

The Reynolds numbers, generally defined as $Re = \rho \bar{u} D / \eta$, were computed for all simulations. The mean velocity \bar{u} through the orifice was approximated as $\bar{u} = Q / AROA$ and as characteristic diameter D , the hydraulic diameter defined by $D = (4 \cdot AROA) / P$, with P the orifice perimeter, was used. In cases with multiple orifices, the overall hydraulic diameter was approximated by

$$D = \frac{\sum_{i=1}^N D_i \cdot AROA_i}{AROA} \quad (6)$$

with D_i and $AROA_i$ the respective hydraulic diameter and area of the i th orifice within a geometry. The Reynolds numbers were thus determined as

$$Re = \frac{\rho \cdot Q \cdot D}{\eta \cdot AROA} \quad (7)$$

2.6. Reduced order model definition, evaluation and application

Based on the results of the regurgitant flow coefficient analysis, we define a shape-based reduced order model of the form (cf. (2)):

$$Q_{ROM} = c_{ROM} \cdot AROA \cdot \sqrt{\Delta p}. \quad (8)$$

The reduced order model flow rate Q_{ROM} describes the model-estimated transient regurgitant flow rate at a transvalvular pressure gradient Δp . The relationship is personalized by an (orifice shape dependent) MR-specific flow coefficient c_{ROM} and the estimated AROA.

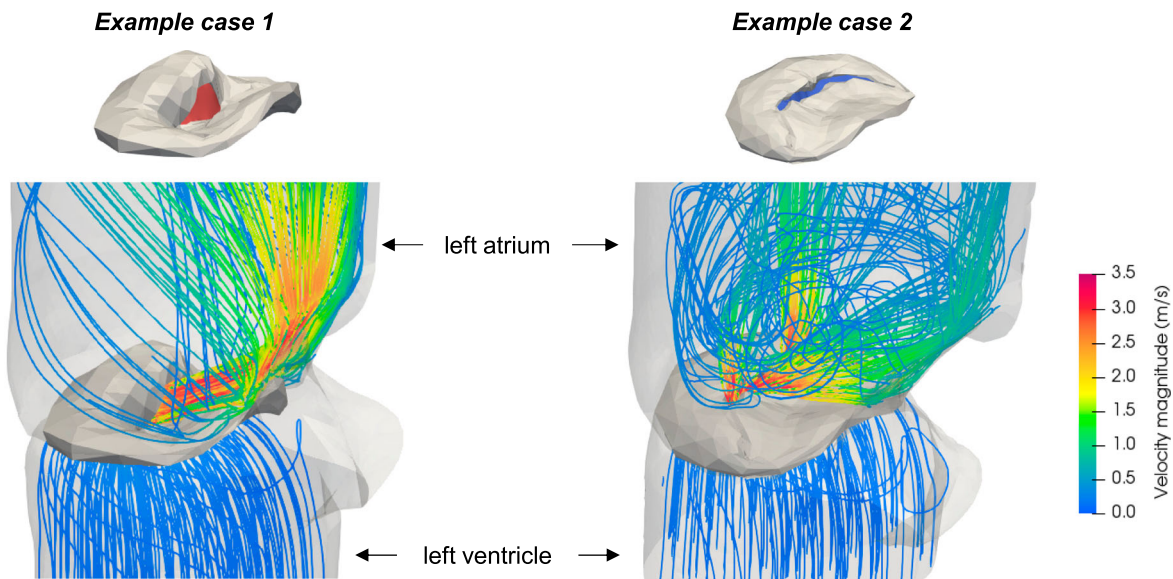


Figure 4. CFD simulated velocity streamlines through regurgitant mitral valves for two example cases at a transvalvular pressure gradient of $\Delta p = 37.5$ mmHg. The blood streams back from the left ventricle into the left atrium. Case 1 shows one eccentric jet, whereas in case 2, there are both central and eccentric jet components.

To compare the shape-based reduced order model performance to the CFD simulation results, we also define a CFD-based model describing the patient-specific pressure gradient-flow rate relationship as

$$\Delta p = a_{1,i}Q + a_{2,i}Q^2 \quad (9)$$

with model parameters $a_{1,i}$ and $a_{2,i}$ fitted individually for each patient i . By re-arranging (9), the CFD-based regurgitant flow rate at any given pressure Δp is thus determined by:

$$Q_{\text{CFD}} = \frac{\sqrt{a_{1,i}^2 + 4a_{2,i}\Delta p} - a_{1,i}}{2a_{2,i}}. \quad (10)$$

The shape-based and CFD-based reduced order model results were compared to determine the accuracy of the shape-based approach both in terms of transient blood flow rate prediction as well as in the determination of the total regurgitant blood volume during one heart cycle, which is a common clinical marker for MR severity. With a given transvalvular pressure gradient curve, the transient blood flow rates during systole can be determined according to (8) and (10), respectively. The regurgitant blood volume can subsequently be computed as the time-integral over the respective estimated blood flow rates.

For the purpose of comparing the shape-based and the CFD-based models, we used the same generic pressure gradient curve as input for each patient. Its shape is based on a best-fit approximation of left ventricular pressure curves of ten patients with MR (not part of the study cohort). We assumed that the transvalvular pressure gradient curve approximately resembles the shape of the left ventricular pressure curve. Furthermore, we used a typical resting heart rate of 60 bpm and a systolic time of 40% of the heart period. The patients included in this study had a mean systolic arterial blood pressure of 135 ± 17 mmHg. Assuming an average elevated left atrial pressure of about 20 mmHg (Maor et al., 2017) in these patients, we chose a maximum pressure gradient of 115 mmHg for the pressure gradient curve.

2.7. Software and data analysis

Data pre-processing and analysis were performed with MATLAB 2019a (The Mathworks, Inc., USA) and Python 3.7 (Python Software Foundation, USA). CFD simulations were performed with Ansys Fluent 19.0 (ANSYS Inc., USA). For the valve orifice estimation and visualization, an implementation of the shrink-wrap algorithm in JavaView (www.javaview.de) was used and manual corrections were done in Meshmixer 3.5 (Autodesk, Inc., USA). Additionally, Paraview 5.6 (Kitware, Inc., USA)

was used for visualization of the segmentation and CFD results. Mean values are reported with their standard deviation as $mean \pm SD$ and median values are denoted as $\tilde{(\cdot)}$. Box plots show median values and interquartile ranges. Linear regression was performed using the least squares approach. If not stated otherwise, variables in equations are considered in the following units as typically used in clinical practice: pressure in mmHg (1 mmHg \approx 133.3 Pa), flow in ml/s, distance in cm and area in cm^2 .

3. Results

3.1. Regurgitant orifice area and shape

The estimated AROA of the 43 studied patients ranged from 0.09 cm^2 to 1.24 cm^2 with a median value of $\tilde{AROA} = 0.39 \text{ cm}^2$, which amounts to about 1-8% of the mitral annulus area in the respective patients (with the exception of one case at 19%). In 23 patients, there was more than one regurgitant orifice, but in only 9 cases the secondary orifices contributed to more than 10% of the total AROA (Figure 5a). A large variation in orifice shapes was observed, as summarized in Table 1 and illustrated in Figure 5b. The orientation ranged from orifices lying mostly parallel to the valve plane (cf. Figure 3) with a maximum orientation index of $I_O = 0.86$, to orifices that were almost perpendicular to the valve plane with a minimum orientation index of $I_O = 0.15$. We found that 18 orifices (42% of cases) were almost planar with a planarity index of $I_P > 0.9$. Ten cases had a planarity index in the lower range of $I_P = 0.57$ to $I_P = 0.69$, indicating a significant amount of curvature in their orifice shape. Half the cases had very elongated orifices with compactness indices of $I_C < 0.21$. To illustrate, a compactness of 0.2 corresponds to an ellipse with an aspect ratio of approximately 12:1. The most compact orifice had a compactness index of $I_C = 0.6$, which corresponds to an elliptic aspect ratio of about 3.5:1. The regurgitant orifice size and shape parameters of all 43 mitral valves are provided as supplemental data to this study.

3.2. MR-specific flow coefficient

A linear regression of the form $Q_{\text{CFD}} = c_{\text{MR}} \cdot AROA \cdot \sqrt{\Delta p_{\text{CFD}}} + \gamma$ was performed to estimate a regurgitant

Table 1. AROA and shape parameter values of regurgitant mitral valve orifices.

Parameter	Value range (median)	Interquartile range
AROA (cm^2)	0.09–1.24 (0.39)	0.25–0.61
Orientation index	0.15–0.86 (0.53)	0.41–0.66
Planarity index	0.57–0.98 (0.84)	0.73–0.94
Compactness index	0.07–0.59 (0.21)	0.16–0.34

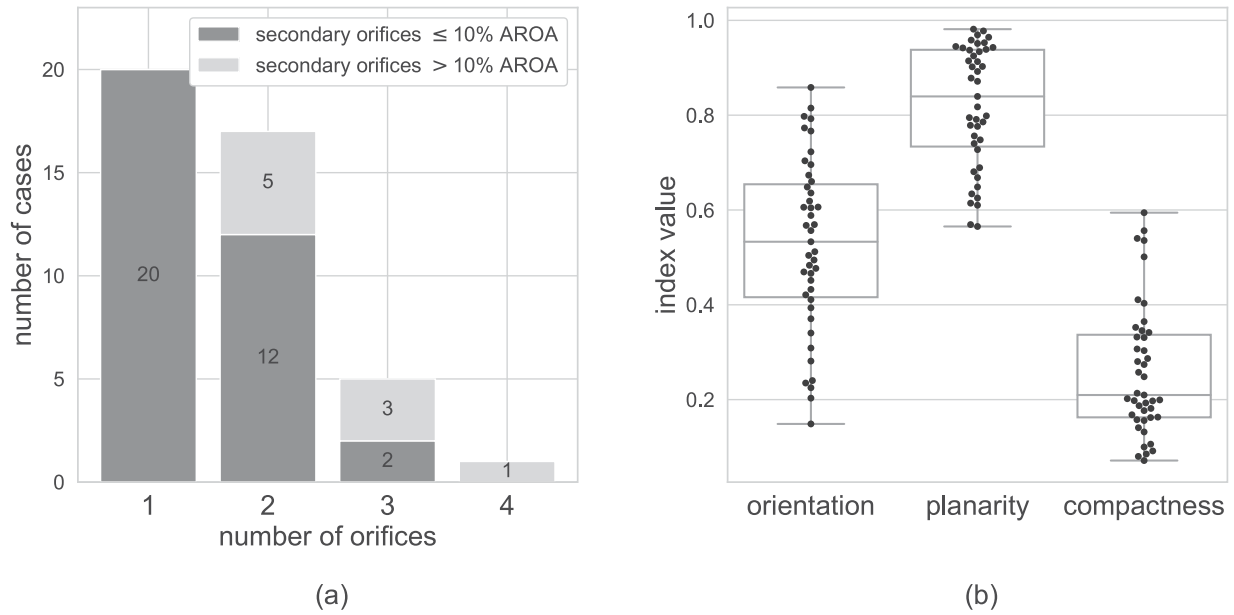


Figure 5. (a) Number of regurgitant orifices within a mitral valve geometry and the contribution of secondary orifices to the total AROA. (b) Dimensionless shape parameter values of the regurgitant mitral valve orifices.

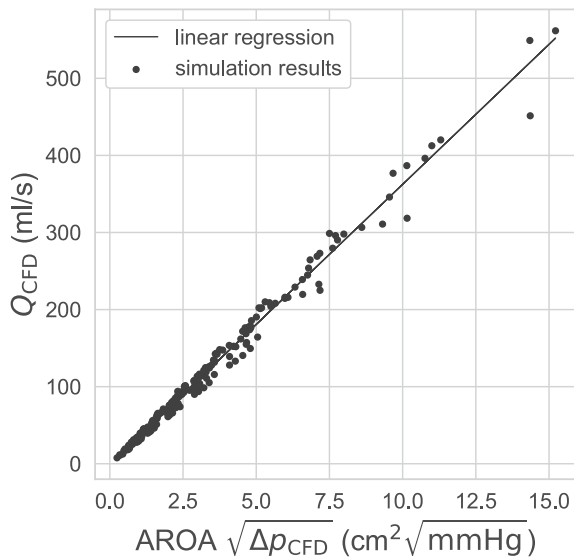


Figure 6. CFD-simulated flow rates Q_{CFD} against the product of the estimated AROA and the square-root of the five different simulated transvalvular pressure gradients Δp_{CFD} for all 43 patients. The slope of the linear regression represents the MR-specific flow coefficient with a value of $c_{MR} = (36.3 \pm 0.3) \text{ cm/s}/\sqrt{\text{mmHg}}$.

mitral valve specific flow coefficient c_{MR} over all 43 patients and five simulations per case (Figure 6). The regression resulted in a high coefficient of determination of $R^2 = 0.99$ with a flow coefficient of $c_{MR} = (36.3 \pm 0.3) \text{ cm/s}/\sqrt{\text{mmHg}}$ and a small and non-significant value ($p = 0.46$) for the intercept of $\gamma = (-0.8 \pm 1.1) \text{ ml/s}$. The root mean square error of the linear regression was $RMSE = 10.5 \text{ ml/s}$ at a mean simulated flow rate of 116 ml/s over all simulations.

3.3. Per-case regurgitant flow coefficients and influence of the Reynolds number

A separate calculation of the flow coefficients for individual cases i and simulations j :

$$c_{i,j} = \frac{Q_{CFD_{i,j}}}{ARO A_i \sqrt{\Delta p_{CFD_j}}} \quad (11)$$

shows that the flow coefficients vary between cases with values ranging from $c = 28.4 \text{ cm/s}/\sqrt{\text{mmHg}}$ to $c = 40.5 \text{ cm/s}/\sqrt{\text{mmHg}}$ (Figure 7a). In addition, there is a noticeable increase in flow coefficients for higher simulated transvalvular pressure gradients, with median values for the flow coefficient increasing from $\tilde{c} = 36.0 \text{ cm/s}/\sqrt{\text{mmHg}}$ for $\Delta p = 7.5 \text{ mmHg}$ to $\tilde{c} = 36.7 \text{ cm/s}/\sqrt{\text{mmHg}}$ for $\Delta p = 150 \text{ mmHg}$. This increase was most pronounced for small orifices ($ARO A < 0.3 \text{ cm}^2$) and cases with $Re < 1000$ at $\Delta p = 7.5 \text{ mmHg}$, as shown in Figure 7b. Reynolds numbers over all simulations ranged from $Re = 203$ to $Re = 8694$, with a median value of $\tilde{Re} = 1813$. For higher Reynolds numbers, the flow coefficients converged to a constant value, that was different for each regurgitant mitral valve. We propose to describe the relationship between the flow coefficient c and the Reynolds number Re for each orifice i individually by

$$c = c_{\infty,i} - \frac{\alpha_i}{Re} \quad (12)$$

with $c_{\infty,i}$ representing the respective limiting flow coefficient at high Reynolds numbers, and α_i describing the slope of the inverse relation with the Reynolds number.

Differences between the fitted approximation using (12) and the flow coefficients computed by (11) were below 1% in all cases.

The fit coefficients α had a positive value in all but two cases and were linearly correlated with the orientation index I_O of the orifices (Figure 7c):

$$\alpha = \beta_0 - \beta_1 \cdot I_O \quad (13)$$

with linear regression coefficients $\beta_0 = (1892 \pm 88)$ cm/s/ $\sqrt{\text{mmHg}}$ and $\beta_1 = (1876 \pm 158)$ cm/s/ $\sqrt{\text{mmHg}}$,

a coefficient of determination of $R^2 = 0.4$ and a root mean square error of $RMSE = 415$ cm/s/ $\sqrt{\text{mmHg}}$.

The flow coefficient may thus be described depending on the orifice orientation and Reynolds number according to:

$$c = c_\infty - \frac{\beta_0 - \beta_1 \cdot I_O}{Re} \quad (14)$$

Figure 7d shows the flow coefficients normalized by their respective c_∞ against the Reynolds numbers divided by the fitted orientation index dependency in (13) for all

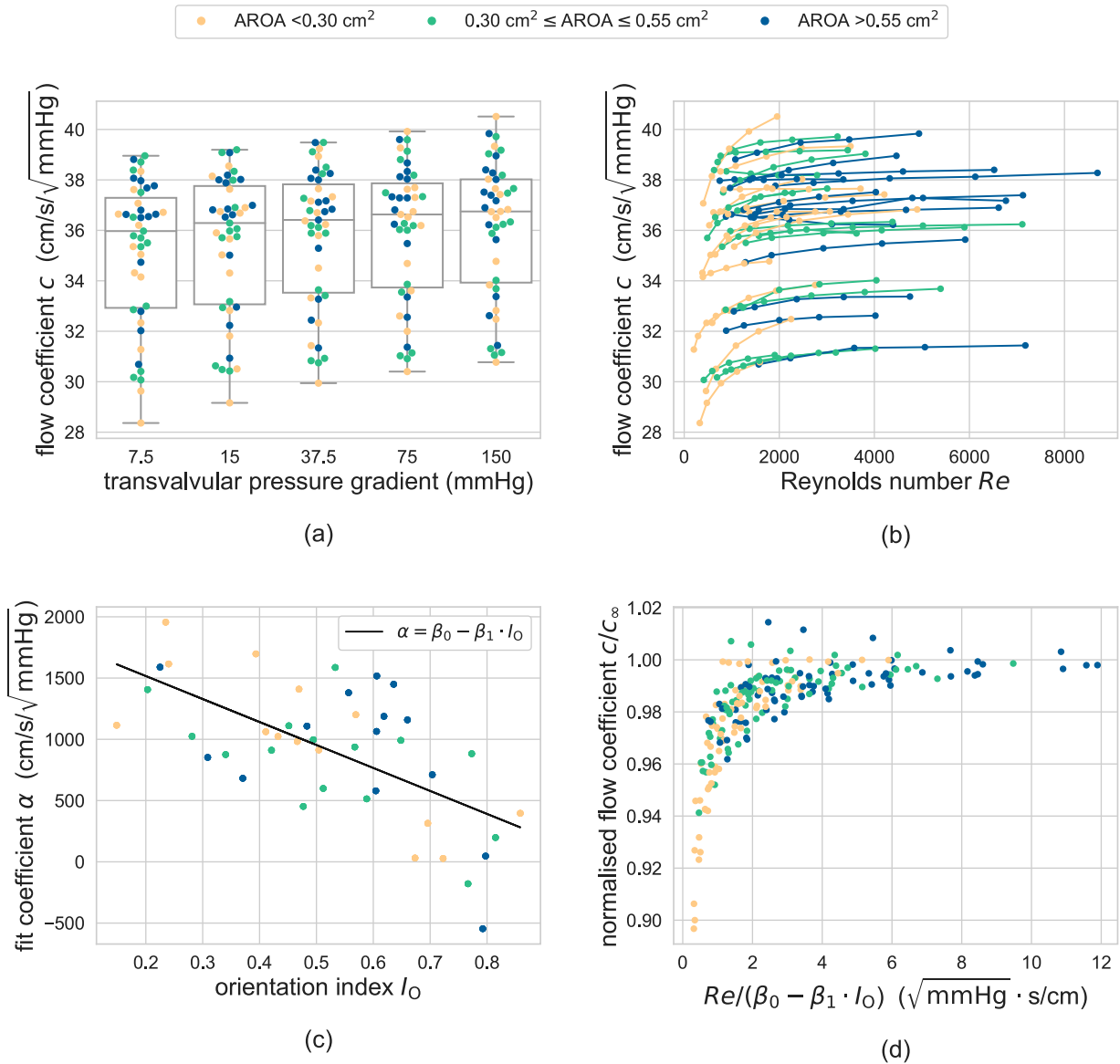


Figure 7. Separate estimation of flow coefficients for each regurgitant mitral valve and simulation shows large variation in flow coefficients between cases. Colors indicate the AROA size of the orifices as categorized into three groups from small (yellow/light) to large (blue/dark). Flow coefficients increase with (a) increasing transvalvular pressure gradient, and (b) increasing Reynolds number, especially at small AROA. Data points belonging to the same mitral valve geometry in (b) are connected by straight lines for illustration purposes. (c) The influence of the Reynolds number on the flow coefficient (expressed by α) was found to be negatively correlated with the orientation index I_O of the orifice. (d) Normalized flow coefficients against Reynolds numbers divided by the fitted orientation index dependency illustrate the convergence of flow coefficients to constant values at large Reynolds numbers and large orifices.

cases and simulations. It illustrates the relative influence of the Reynolds number (adjusted by the specific orifice orientation of each mitral valve geometry) on the flow coefficient. The maximum influence of the Reynolds number on the flow coefficient was observed for cases with small AROA and small Reynolds number, for which the flow coefficient was in the order of 90% of the limiting flow coefficient c_∞ . This influence decreased quickly with increasing Reynolds number, with less than four percentage points difference between the flow coefficients and their respective c_∞ for cases with $\text{AROA} > 0.55 \text{ cm}^2$. Overall, the contribution of the Reynolds number to the total variation in flow coefficients is small compared to the contribution of differences in c_∞ between cases. Values of c_∞ range from $31.3 \text{ cm/s}/\sqrt{\text{mmHg}}$ to $41.2 \text{ cm/s}/\sqrt{\text{mmHg}}$ and will be analysed further in the following section.

3.4. Influence of orifice shape on the flow coefficient

Regarding the differences in flow coefficients between the orifices, no conclusive relationships between individual shape parameters and the flow coefficients could be established. However, considering the combination of the orientation and compactness indices of the orifices together with the fitted flow coefficients at large Reynolds numbers c_∞ (Figure 8a), one can see that larger coefficients are primarily found for orifices with low compactness and an orientation parallel to the valve plane (high orientation index). This may suggest a distinction of regurgitant mitral valves into two shape groups: those with low compactness, oriented parallel to the valve plane and those with higher compactness that are oriented more perpendicular to the valve plane. Logistic regression was used to find the optimal separation of the two shape groups based on c_∞ , which resulted in a separation line of:

$$s = 0.47 \cdot I_C + 0.33 \quad (15)$$

as shown in Figure 8a.

After assigning each case to its shape group using (15) as separation, a linear regression was performed separately for the cases of each shape group (Figure 8b). The first group with high compactness and low orientation indices resulted in a flow coefficient of $c_{\text{MR},1} = (32.3 \pm 0.3) \text{ cm/s}/\sqrt{\text{mmHg}}$ and a small intercept of $\gamma_1 = (3.0 \pm 1.4) \text{ ml/s}$ with a coefficient of determination of $R^2 = 0.99$ and a root mean square error of $\text{RMSE} = 6.9 \text{ ml/s}$. The second group with low compactness and high orientation indices resulted in $c_{\text{MR},2} = (37.6 \pm 0.2) \text{ cm/s}/\sqrt{\text{mmHg}}$ and $\gamma_2 = (-1.6 \pm 0.8) \text{ ml/s}$ with $R^2 = 0.99$ and $\text{RMSE} = 6.3 \text{ ml/s}$.

3.5. Orifice shape-based reduced order model definition

In the previous sections, we investigated the flow coefficients of regurgitant mitral valves in order to develop a reduced order model of the form (8) to describe the patient-specific blood pressure gradient-flow rate relationship during MR. Starting from a model using a common MR-specific flow coefficient for all patients based on a linear regression analysis, we stepwise refined the model, taking into account both the influence of the Reynolds number and the orifice shape of an individual regurgitant mitral valve. We therewith developed three possible ways of defining the flow coefficient. The respective reduced order models will be referred to as ROM1 to ROM3 and are defined below.

ROM1: A common (constant) flow coefficient is chosen for all regurgitant mitral valves, based on the linear regression result (while neglecting the non-significant intercept):

$$c_{\text{ROM1}} = c_{\text{MR}} = 36.3 \frac{\text{cm}}{\text{s} \cdot \sqrt{\text{mmHg}}} \quad (16)$$

ROM2: The common flow coefficient used in ROM1 is now adjusted for the orifice shape-specific Reynolds number dependency (cf. (14)):

$$c_{\text{ROM2}} = c_{\text{MR}} - \frac{\beta_0 - \beta_1 \cdot I_O}{Re} \quad (17)$$

with model coefficients β_0 and β_1 , patient-specific orientation index I_O and Reynolds number Re . The flow coefficient c_{ROM2} as defined by (17) is flow-dependent due to the flow dependence of the Reynolds number as computed by (7). To obtain a flow-independent definition of c_{ROM2} , (17) and (7) were inserted in the shape-based reduced order model equation (8), which was subsequently solved for Q . This led to the following flow-independent definition of

$$c_{\text{ROM2}}(\Delta p, I_O, D) = \frac{1}{2} \cdot c_{\text{MR}} \left(1 + \sqrt{1 - \frac{4\eta}{\rho} \cdot \frac{\beta_0 - \beta_1 \cdot I_O}{c_{\text{MR}}^2 \cdot D \cdot \sqrt{\Delta p}}} \right), \quad (18)$$

with $4\eta/\rho \approx 0.15 \text{ cm}^2/\text{s}$ for blood. The flow coefficient in ROM2 thus depends on the transvalvular pressure gradient Δp , as well as on the shape of the orifice, described by the orientation index I_O and the hydraulic diameter D (in cm).

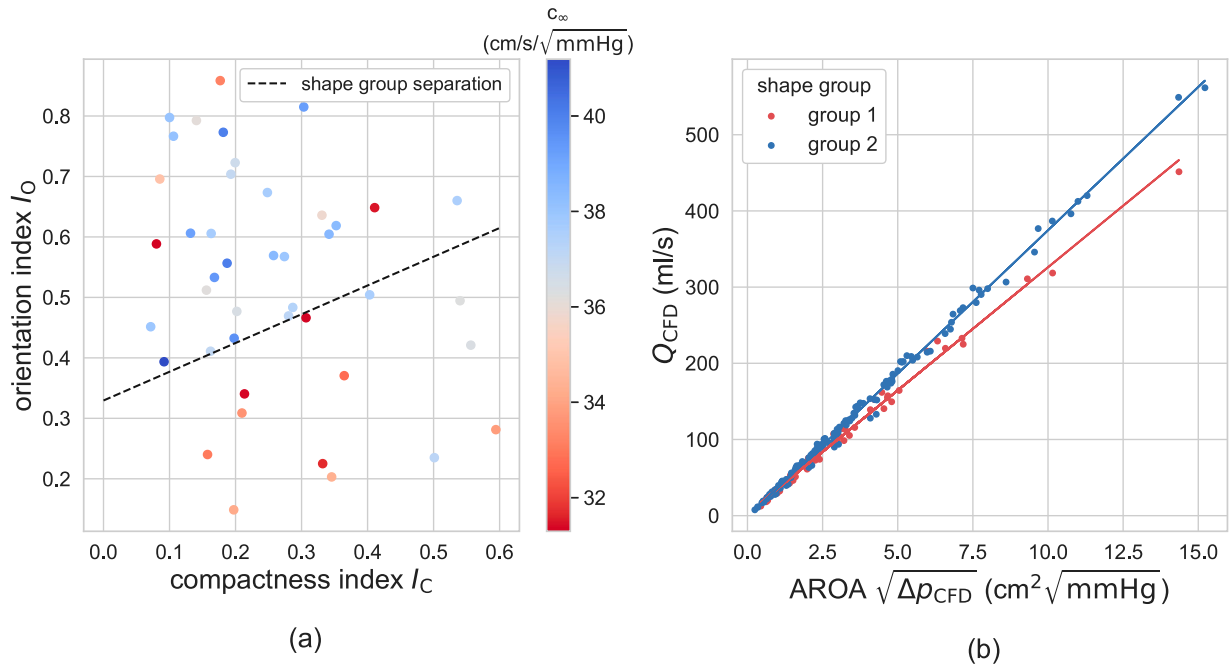


Figure 8. (a) Separation of regurgitant mitral valve cases into two shape groups according to their orientation and compactness indices. Each case is represented by a dot colored by the value of their flow coefficient at high Reynolds numbers, c_{∞} . The dashed line shows the logistic regression-based separation of the cases into two different shape groups: Cases with larger flow coefficients showed lower compactness and higher orientation indices (blue) as opposed to those with smaller flow coefficients (red). (b) Separate linear regressions were performed for the cases of the two shape groups defined in (a), which resulted in a lower overall flow coefficient in group 1 compared to group 2.

ROM3: ROM3 uses the definition of ROM2 in (18) and adds a distinction between two shape groups, such that

$$c_{MR} = c_{MR}(I_O, I_C) = \begin{cases} c_{MR,1} = 32.3 \frac{\text{cm}}{\text{s}\sqrt{\text{mmHg}}} & \text{for } I_O \leq 0.47 \cdot I_C + 0.33 \\ c_{MR,2} = 37.6 \frac{\text{cm}}{\text{s}\sqrt{\text{mmHg}}} & \text{for } I_O > 0.47 \cdot I_C + 0.33 \end{cases} \quad (19)$$

while again, neglecting the small intercepts in the linear regression result of both shape groups.

3.6. Comparison between orifice shape-based and CFD-based reduced order models

Figure 9 shows Bland–Altman plots to compare the orifice shape-based ROM1 to ROM3 with the CFD-based reduced order model (cf. (10)) regarding the prediction of transient regurgitant blood flow rates and total regurgitant blood volumes. Blood flow rates for each patient in Figure 9a-c were computed for the five respective pressure gradients used in the CFD simulations. Regurgitant blood volumes (RV) in Figure 9d-f were computed using the pressure gradient curve displayed in Figure 10a with a maximum pressure gradient of 115 mmHg.

The additional consideration of the pressure gradient and valve shape in the computation of the flow coefficient

in ROM2 led to a more pressure-independent difference between orifice shape-based and CFD-based estimated flow rates as compared to ROM1 (Figure 9a-b). However, this only had a minor effect on the estimated regurgitant blood volumes (Figure 9d-e). With the exception of one case, the regurgitant volume estimations of both ROM1 and ROM2 differ by less than 10 ml from the CFD-based estimation.

The consideration of two separate shape groups in ROM3 reduces this difference to less than 6 ml in 90% of the cases. Larger relative differences between ROM3 and CFD-based flow rate estimations above 10% are observed for cases with smaller AROA and thus small flow rates, leading to small absolute differences in flow rate prediction.

3.7. Shape-based ROM3: application examples

We defined four theoretical cases with different AROA size and shape group as summarized in Table 2 to illustrate the effect of orifice size, shape and transvalvular pressure gradient on the regurgitant flow rates and volumes. For each case, the transient flow rates and respective regurgitant volumes were computed using the pressure curves shown in Figure 10a with three different maximum transvalvular pressure gradients of 100,

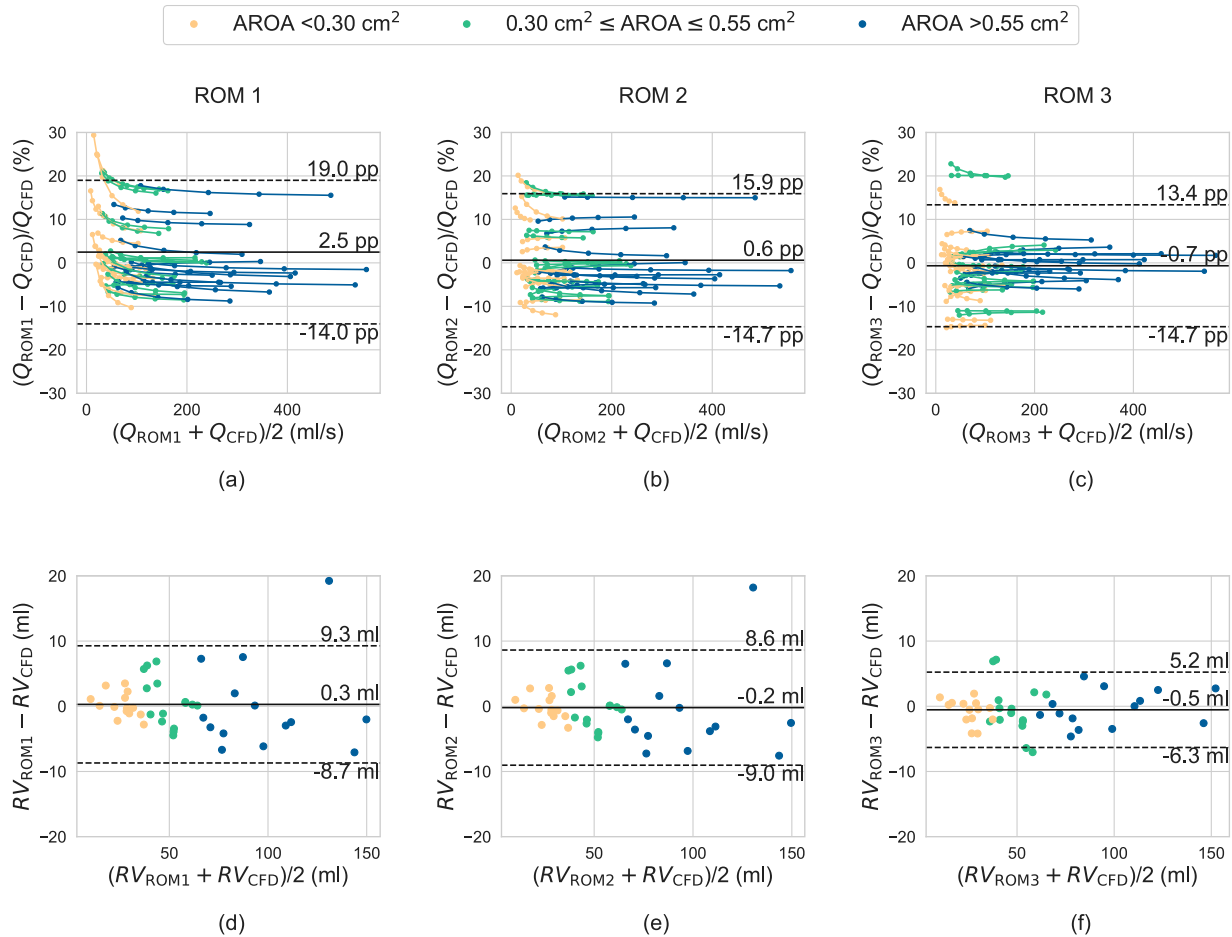


Figure 9. Comparison between the estimations made by the three reduced order models ROM1 to ROM3 and the CFD results regarding (a-c) the transient blood flow rates and (d-f) the total regurgitant volume (RV). Displayed for each figure are mean bias and 95% limits of agreement. Data points belonging to the same mitral valve geometry in (a-c) are connected by straight lines for illustration purposes.

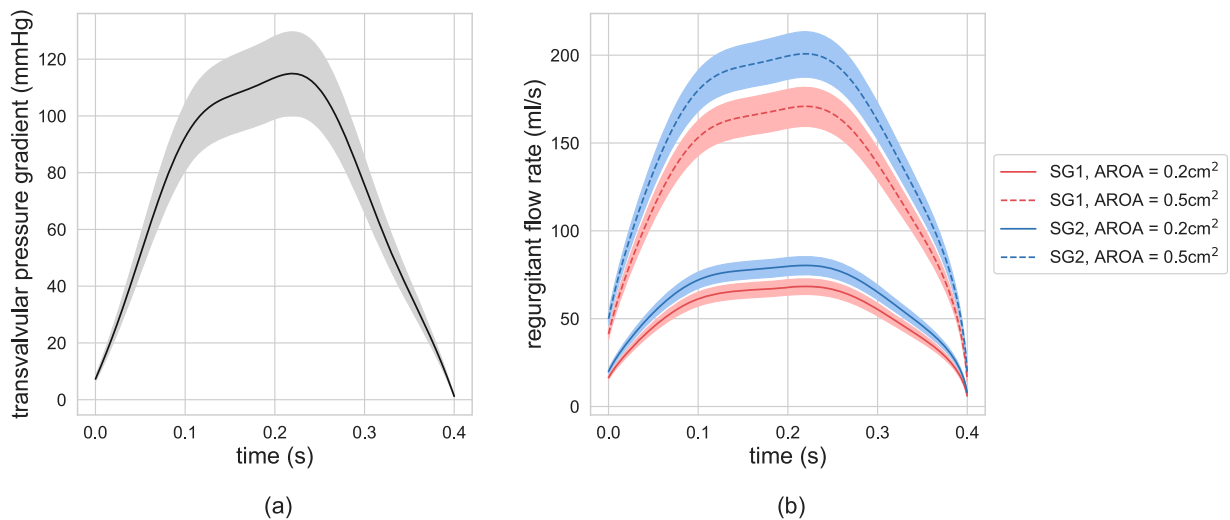


Figure 10. (a) Averaged transvalvular pressure gradient curve during the systolic phase with a maximum pressure gradient of 115 mmHg. The range between curves with maximum pressure gradients of 100 and 130 mmHg is indicated in grey. (b) Estimated transient flow rates using ROM3 and the pressure gradient curves in (a) as input for the four example cases listed in Table 2.

Table 2. Theoretical example cases of regurgitant orifices of different shapes and sizes. Regurgitant volumes were computed with ROM3 using pressure gradient curves with maximum values of 100, 115 and 130 mmHg as input.

Case	AROA (cm ²)	Shape group	l_o	l_c	Regurgitant volumes (ml) for pressure gradient curves with maximum values of		
					100 mmHg	115 mmHg	130 mmHg
1	0.2	SG1	0.3	0.5	19.7	21.1	22.4
2	0.2	SG2	0.7	0.2	23.2	24.9	26.4
3	0.5	SG1	0.3	0.5	49.2	52.8	56.1
4	0.5	SG2	0.7	0.2	58.0	62.2	66.1

115 and 130 mmHg. The resulting flow curves are shown in Figure 10b and the regurgitant volumes are listed in Table 2. Regurgitant volumes for the two orifices in shape group 1 are about 15% smaller compared to those in shape group 2 with the same respective orifice area. An increase of the maximum pressure gradient from 100 mmHg to 130 mmHg increased the regurgitant volumes by about 14%.

4. Discussion

In this work, we developed a reduced order model to quantify the regurgitant flow rate through patient-specific mitral valves at a given transvalvular pressure gradient. The reduced order model is parameterized by the patient-specific AROA, as well as by a MR-specific flow coefficient. For this flow coefficient, three implementations with increasing complexity were evaluated, from a constant coefficient for all cases to a coefficient that depends on both the Reynolds number and the regurgitant orifice shape.

To determine the AROA for the 43 MR patients included in this study, we proposed the use of a shrink-wrap-based algorithm to be applied to the segmented geometries of the regurgitant mitral valves. The method enabled a detailed representation of the often complex regurgitant orifice shape in 3D space and was equally applicable to all MR patients. This exceeds the capabilities of standard clinical methods for estimating the regurgitant orifice area, which only estimate an effective area without its explicit shape, or a 2D projection, and which can be unreliable in patients with complex orifice shapes (Biner et al., 2010; Coisne et al., 2020). Our shape analysis demonstrated a large morphological variety between regurgitant orifices in terms of planarity, compactness and orientation relative to the valve plane. Even though we lack a ground truth for the actual anatomic orifice area and shape, the shrink-wrap-based method is rather robust with a coefficient of variation in the order of 2%. At the current time, however, the method is more time expensive than standard clinical assessments, since

it requires accurate segmentation of the regurgitant valve as well as several manual steps during the shrink-wrap procedure. For application in a clinical setting, further automation in this regard will be required.

CFD simulations of blood flow through the regurgitant mitral valve geometries were used to determine the regurgitant blood flow rate at different pressure gradients across the valves. Combination of these results with the AROA estimations enabled the computation of flow coefficients for each valve and simulation. Despite a large variability in flow coefficients between cases, the usage of a common MR-specific flow coefficient of $c_{MR} = 36.3 \text{ cm/s}/\sqrt{\text{mmHg}}$ for all patients in the reduced order model ROM1 resulted in a good agreement between ROM1 and CFD predicted regurgitant volumes with a limit of agreement of 9 ml.

Our analysis of the CFD results showed a small increase in flow coefficient with increasing Reynolds number for $Re < 2000$. This is also observed for flow through different types of flow meters, which are comparable in their geometry to our simulation setup (Abd et al., 2019; Hollingshead et al., 2011). We found that the influence of the Reynolds number on the flow coefficient is inversely correlated with the orientation index of the regurgitant orifice. This Reynolds number dependency was accounted for in ROM2, but it contributed little to the model performance in terms of predicted regurgitant volumes. The reason for this is that it mainly affected the flow rate at low pressure gradients and small orifice areas. The agreement between reduced order model and CFD simulations was, however, increased with ROM3, in which the orifices were separated into two shape groups and group-specific flow coefficients were applied. The limit of agreement between ROM3 and CFD estimated regurgitant volumes reduced to 5.7 ml. At a mean regurgitant volume of $RV = 57 \text{ ml}$ over all cases, this corresponds to an error of 10%. In comparison, the inter-observer variability in regurgitant volume estimations in clinical practice using echocardiography is reported with limits of agreement in the order of 15 ml and higher (Cawley et al., 2013; Lopez-Mattei et al., 2016; Thavendiranathan et al., 2013).

Although the investigated orifice shape parameters could not fully explain the inter-valve differences in flow coefficients, the usage of the AROA and the distinction into two shape groups are a promising route for personalized reduced order models of MR in clinical practice. Depending on the aetiology and resulting morphology of the diseased valve (e.g. annulus dilatation, prolapsed or flail leaflets), different flow coefficients may be applicable to accurately predict the regurgitant flow rate. This is also supported by the results of a CFD study by This et al. (2020), who found the mitral valve

shape to be an important determinant of regurgitant blood flow. For valves with an elongated orifice shape that is oriented more parallel to the valve plane (shape group 2), the determined flow coefficient in our study was with $c_{MR,2} = 37.6 \text{ cm/s}/\sqrt{\text{mmHg}}$ remarkably close to the flow coefficient for mitral valve stenosis of $c_{MS} = 37.9 \text{ cm/s}/\sqrt{\text{mmHg}}$ (Cohen & Gorlin, 1972), despite the difference in disease characteristics and flow direction. The shape of stenotic mitral orifices in terms of their orientation and compactness is often similar to that of the regurgitant orifices in shape group 2 (Krapf et al., 2013), which supports our finding of similar flow coefficients. Valves of shape group 1 with more compact orifice shapes and more perpendicular orientation with respect to the valve plane, had a significantly lower flow coefficient of $c_{MR,1} = 32.3 \text{ cm/s}/\sqrt{\text{mmHg}}$. This corresponds to an about 15% lower regurgitant flow rate at the same orifice area and transvalvular pressure gradient compared to group 2 valves. Due to the angle between the valve plane and the orifice plane in shape group 1, the regurgitant jet streams closer to the wall, leading to a lower flow coefficient in comparison to shape group 2 valves. This correlates well with findings of differences between free and wall turbulent jets (Aloysius & Wrobel, 2009).

In this study, we demonstrated the applicability of the reduced order model approach by computing regurgitant volumes using the same generic transvalvular pressure gradient curve for each patient. However, for a full patient-specific evaluation, personalized transient pressure gradient curves are required. Lumped parameter models of the human circulation can be used to simulate these transient pressure curves patient-specifically using non-invasive clinical measurements for personalization (Itu et al., 2014; Meiburg et al., 2020; Pant et al., 2017). Integrating the regurgitation model into a lumped parameter model can thus provide an alternative method for personalized computation of MR in the clinic and can be used to evaluate the effect of MR treatment on the heart's hemodynamics.

The in-silico approach of estimating the flow coefficients based on CFD simulations and orifice area estimations has distinct advantages, such as a controlled and reproducible setup that cannot be achieved in a clinical setting, but the method also faces several limitations. In this study, we only considered regurgitation at a single time point during systole and have thus neglected transient flow effects and in particular the soft tissue properties of the valve leaflets and their interactions with the fluid. With that we have also assumed that a constant AROA at the simulated time point is representative for the entire systolic phase, which may not be true in all patients. Time-varying mitral valve area is well known for both phases of the heart cycle: diastole (Mynard et al.,

2012) and systole in the case of MR (Schwammenthal et al., 1994). Presuming AROA segmentation in time-dependent 3D TEE imaging data for each time step of the systolic phase, the impact of the time-varying AROA for the calculation of the regurgitation volume can be easily incorporated by an integration over time in a same way as it was demonstrated for the time-varying transvalvular pressure difference in this study. Furthermore, a transient CFD simulation with fluid structure interaction may provide further insight into the relationship between the regurgitant flow coefficient and the orifice shape over the entire regurgitation phase. Inaccuracies in the estimated orifice area with respect to the unknown 'true' value, as well as unphysiologically sharp edges in the segmented geometries of the mitral valve leaflets, which may reduce the simulated flow rate, are both additional sources of uncertainty in the estimation of the flow coefficients.

5. Conclusion

A reduced order model predicting regurgitant mitral valve flow was developed using steady-state CFD simulations, estimations of the AROA in 3D space and dimensionless orifice shape parameters. The model is parameterized by the AROA and its shape parameters, which can be accurately estimated from TEE-based reconstructions of the regurgitant mitral valve using a shrink-wrap algorithm. The integration of the proposed reduced order model into a patient-specific lumped parameter model of the human circulation may provide an easy and fast way to simulate and quantify MR in individual patients. Due to several limitations of the present study, including the number of investigated cases and the use of steady-state flow simulations at a single time point during the cardiac cycle, the proposed reduced order model should be considered with caution. Prior to the translation of the developed model into clinical routine, a clinical validation study including the enrollment of new patient data is required. Depending on the results of the clinical study, the future focus of the methodological development could involve the incorporation of fluid-structure interaction into the CFD approach.

Acknowledgement

We acknowledge support from the German Research Foundation (DFG) and the Open Access Publication Fund of Charité - Universitätsmedizin Berlin.

Data availability statement

The reconstructed regurgitant mitral valve geometries used in this study are made publicly available at

<https://doi.org/10.6084/m9.figshare.14393600>. The simulated regurgitant flow rates, as well as the shape properties of the regurgitant orifices are provided as supplemental data.

Disclosure statement

No potential conflict of interest was reported by the author(s).

Funding

This project was partially funded by the European Union's Horizon 2020 programme H2020-EU.3.1.5., grant agreement no. 689617 (EurValve project).

ORCID

J. Franz  <http://orcid.org/0000-0001-7443-0079>

References

- Abd, H. M., Alomar, O. R., & Mohamed, I. A. (2019). Effects of varying orifice diameter and Reynolds number on discharge coefficient and wall pressure. *Flow Measurement and Instrumentation*, 65(January), 219–226. <https://doi.org/10.1016/j.flowmeasinst.2019.01.004>
- Aftab, S. M. A., Rafie, A. S. M., Razak, N. A., & Ahmad, K. A. (2016). Turbulence model selection for low Reynolds number flows. *PLoS ONE*, 11(4), 1–15. <https://doi.org/10.1371/journal.pone.0153755>
- Aloysius, S. S., & Wrobel, L. C. (2009). Comparison of flow and dispersion properties of free and wall turbulent jets for source dynamics characterisation. *Environmental Modelling and Software*, 24(8), 926–937. <https://doi.org/10.1016/j.envsoft.2008.12.007>
- Athar, M., Ansari, M. A., & Khan, M. A. (2003). Flow characteristics of elliptical orifice plates. *ISH Journal of Hydraulic Engineering*, 9(2), 22–35. <https://doi.org/10.1080/09715010.2003.10514731>
- Baumgartner, H., Falk, V., Bax, J. J., De Bonis, M., Hamm, C., Holm, P. J., Iung, B., Lancellotti, P., Lansac, E., Rodriguez Muñoz, D., Rosenhek, R., Sjögren, J., Tornos Mas, P., Vahanian, A., Walther, T., Wendler, O., Windecker, S., Zamorano, J. L., Roffi, M., ... Brecker, S. J. D. (2017). 2017 ESC/EACTS guidelines for the management of valvular heart disease. *European Heart Journal*, 38(36), 2739–2791. <https://doi.org/10.1093/eurheartj/ehx391>
- Bianchi, M., Marom, G., Ghosh, R. P., Rotman, O. M., Parikh, P., Gruberg, L., & Bluestein, D. (2019). Patient-specific simulation of transcatheter aortic valve replacement: impact of deployment options on paravalvular leakage. *Biomechanics and Modeling in Mechanobiology*, 18(2), 435–451. <https://dx.doi.org/10.1007/s10237-018-1094-8>
- Biner, S., Rafique, A., Rafi, F., Tolstrup, K., Noorani, O., Shiota, T., Gurudevan, S., & Siegel, R. J. (2010). Reproducibility of proximal isovelocity surface area, Vena Contracta, and regurgitant Jet area for assessment of mitral regurgitation severity. *JACC: Cardiovascular Imaging*, 3(3), 235–243. <https://doi.org/10.1016/j.jcmg.2009.09.029>
- Bubak, M., Czechowicz, K., Gubała, T., Hose, D. R., Kasztelnik, M., Malawski, M., Meizner, J., Nowakowski, P., & Wood, S. (2021). The EurValve model execution environment. *Interface Focus*, 11(1), <https://doi.org/10.1098/rsfs.2020.0006rsfs20200006>
- Buchner, S., Poschenrieder, F., Hamer, O. W., Jungbauer, C., Resch, M., Birner, C., Fellner, C., Riegger, G. A., Stroszczynski, C., Djavidani, B., Debl, K., & Luchner, A. (2011). Direct visualization of regurgitant orifice by CMR reveals differential asymmetry according to etiology of mitral regurgitation. *JACC: Cardiovascular Imaging*, 4(10), 1088–1096. <https://doi.org/10.1016/j.jcmg.2011.06.020>
- Cawley, P. J., Hamilton-Craig, C., Owens, D. S., Krieger, E. V., Strugnell, W. E., Mitsumori, L., D'Jang, C. L., Schwae-gler, R. G., Nguyen, K. Q., Nguyen, B., Maki, J. H., & Otto, C. M. (2013). Prospective comparison of valve regurgitation quantitation by cardiac magnetic resonance imaging and transthoracic echocardiography. *Circulation: Cardiovascular Imaging*, 6(1), 48–57. <https://doi.org/10.1161/CIRCIMAGING.112.975623>
- Chandra, S., Salgo, I. S., Sugeng, L., Weinert, L., Settlemier, S. H., Mor-Avi, V., & Lang, R. M. (2011). A three-dimensional insight into the complexity of flow convergence in mitral regurgitation: Adjunctive benefit of anatomic regurgitant orifice area. *American Journal of Physiology-Heart and Circulatory Physiology*, 301(3), H1015–H1024. <https://doi.org/10.1152/ajpheart.00275.2011>
- Cherry, E. M., & Eaton, J. K. (2013). Shear thinning effects on blood flow in straight and curved tubes. *Physics of Fluids*, 25(7), <https://doi.org/10.1063/1.4816369>
- Cohen, M. V., & Gorlin, R. (1972). Modified orifice equation for the calculation of mitral valve area. *American Heart Journal*, 84(6), 839–840. [https://doi.org/10.1016/0002-8703\(72\)90080-4](https://doi.org/10.1016/0002-8703(72)90080-4)
- Coisne, A., Aghezzaf, S., Edmé, J. L., Bernard, A., Ma, I., Bohbot, Y., Di Lena, C., Nicol, M., Lavie Badie, Y., Eyharts, D., Seemann, A., Falaise, C., Ternacle, J., Nguyen, A., Montier, G., Hubert, A., Montaigne, D., Donal, E., & Dreyfus, J. (2020). Reproducibility of reading echocardiographic parameters to assess severity of mitral regurgitation. Insights from a French multicentre study. *Archives of Cardiovascular Diseases*, 113(10), 599–606. <https://doi.org/10.1016/j.acvd.2020.02.004>
- Doost, S. N., Ghista, D., Su, B., Zhong, L., & Morsi, Y. S. (2016). Heart blood flow simulation: A perspective review. *BioMedical Engineering OnLine*, 15(1), 101. <https://doi.org/10.1186/s12938-016-0224-8>
- El-Tallawi, K. C., Messika-Zeitoun, D., & Zoghbi, W. A. (2017). Assessment of the severity of native mitral valve regurgitation. *Progress in Cardiovascular Diseases*, 60(3), 322–333. <https://doi.org/10.1016/j.pcad.2017.11.005>
- Flachskampf, F. A., Weyman, A. E., Guerrero, J. L., & Thomas, J. D. (1990). Influence of orifice geometry and flow rate on effective valve area: An in vitro study. *Journal of the American College of Cardiology*, 15(5), 1173–1180. [https://doi.org/10.1016/0735-1097\(90\)90260-V](https://doi.org/10.1016/0735-1097(90)90260-V)
- Gilon, D., Cape, E. G., Handschumacher, M. D., Song, J.-K., Solheim, J., VanAuker, M., King, M. E. E., & Levine, R. A. (2002). Effect of three-dimensional valve shape on the hemodynamics of aortic stenosis. *Journal of the American College of Cardiology*, 40(8), 1479–1486. [https://doi.org/10.1016/S0735-1097\(02\)02269-6](https://doi.org/10.1016/S0735-1097(02)02269-6)
- Gorlin, R., & Gorlin, S. G. (1951). Hydraulic formula for calculation of the area of the stenotic mitral valve, other cardiac

- valves, and central circulatory shunts. I. *American Heart Journal*, 41(1), 1–29. [https://doi.org/10.1016/0002-8703\(51\)90002-6](https://doi.org/10.1016/0002-8703(51)90002-6)
- Hinghofer-Szalkay, H., Kenner, T., Leopold, H., & Holzer, H. (1979). Die anwendung der biegeschwinger methode zur messung von blutdicke und hämatokrit. *Klinische Wochenschrift*, 57(21), 1163–1167. <https://doi.org/10.1007/BF01491756>
- Hollingshead, C. L., Johnson, M. C., Barfuss, S. L., & Spall, R. E. (2011). Discharge coefficient performance of venturi, standard concentric orifice plate, V-cone and wedge flow meters at low Reynolds numbers. *Journal of Petroleum Science and Engineering*, 78(3–4), 559–566. <https://doi.org/10.1016/j.petrol.2011.08.008>
- Huttary, R., Goubergrits, L., Schütte, C., & Bernhard, S. (2017). Simulation, identification and statistical variation in cardiovascular analysis (SISCA) – A software framework for multi-compartment lumped modeling. *Computers in Biology and Medicine*, 87, 104–123. <https://doi.org/10.1016/j.compbiomed.2017.05.021>
- Itu, L., Sharma, P., Georgescu, B., Kamen, A., Suci, C., & Comaniciu, D. (2014). *Model based non-invasive estimation of PV loop from echocardiography*. 2014 36th annual International Conference of the IEEE Engineering in Medicine and Biology society, EMBC 2014, 6774–6777. <https://doi.org/10.1109/EMBC.2014.6945183>
- Itu, L., Sharma, P., Ralovich, K., Mihalef, V., Ionasesc, R., Everett, A., Ringel, R., Kamen, A., & Comaniciu, D. (2013). Non-invasive hemodynamic assessment of aortic coarctation: Validation with in vivo measurements. *Annals of Biomedical Engineering*, 41(4), 669–681. <http://dx.doi.org/10.1007/s10439-012-0715-0>
- Iung, B., Baron, G., Tornos, P., Gohlke-Bärwolf, C., Butchart, E. G., & Vahanian, A. (2007). Valvular heart disease in the community: A European experience. *Current Problems in Cardiology*, 32(11), 609–661. <https://doi.org/10.1016/j.cpcardi.2007.07.002>
- Kang, T., Mukherjee, D., Kim, J. M., Park, K. Y., & Ryu, J. (2021). Effects of progressive carotid stenosis on cerebral haemodynamics: Aortic-cerebral 3D patient-specific simulation. *Engineering Applications of Computational Fluid Mechanics*, 15(1), 830–847. <https://doi.org/10.1080/19942060.2021.1916601>
- Krapf, L., Dreyfus, J., Cueff, C., Lepage, L., Brochet, É, Vahanian, A., & Messika-Zeitoun, D. (2013). Anatomical features of rheumatic and non-rheumatic mitral stenosis: Potential additional value of three-dimensional echocardiography. *Archives of Cardiovascular Diseases*, 106(2), 111–115. <https://doi.org/10.1016/j.acvd.2012.11.004>
- Lopez-Mattei, J. C., Ibrahim, H., Shaikh, K. A., Little, S. H., Shah, D. J., Maragiannis, D., & Zoghbi, W. A. (2016). Comparative assessment of mitral regurgitation severity by transthoracic echocardiography and cardiac magnetic resonance using an integrative and quantitative approach. *American Journal of Cardiology*, 117(2), 264–270. <https://doi.org/10.1016/j.amjcard.2015.10.045>
- Maor, E., Raphael, C. E., Panaich, S. S., Reeder, G. S., Nishimura, R. A., Nkomo, V. T., Rihal, C. S., & Eleid, M. F. (2017). Acute changes in left atrial pressure after MitraClip Are associated with improvement in 6-minute walk distance. *Circulation: Cardiovascular Interventions*, 10(4), 1–7. <https://doi.org/10.1161/CIRCINTERVENTIONS.116.004856>
- Meiburg, R., Huberts, W., Rutten, M. C. M., & van de Vosse, F. N. (2020). Uncertainty in model-based treatment decision support: Applied to aortic valve stenosis. *International Journal for Numerical Methods in Biomedical Engineering*, 36(10), 1–21. <https://doi.org/10.1002/cnm.3388>
- Mittal, R., Seo, J. H., Vedula, V., Choi, Y. J., Liu, H., Huang, H. H., Jain, S., Younes, L., Abraham, T., & George, R. T. (2016). Computational modeling of cardiac hemodynamics: Current status and future outlook. *Journal of Computational Physics*, 305(2), 1065–1082. <https://doi.org/10.1016/j.jcp.2015.11.022>
- Mynard, J. P., Davidson, M. R., Penny, D. J., & Smolich, J. J. (2012). A simple, versatile valve model for use in lumped parameter and one-dimensional cardiovascular models. *International Journal for Numerical Methods in Biomedical Engineering*, 28(6–7), 626–641. <https://doi.org/10.1002/cnm.1466>
- Nishimura, R. A., Otto, C. M., Bonow, R. O., Carabello, B. A., Erwin, J. P., Fleisher, L. A., Jneid, H., Mack, M. J., McLeod, C. J., O’Gara, P. T., Rigolin, V. H., Sundt, T. M., & Thompson, A. (2017). 2017 AHA/ACC focused update of the 2014 AHA/ACC Guideline for the management of patients With valvular heart disease. *Journal of the American College of Cardiology*, 70(2), 252–289. <https://doi.org/10.1016/j.jacc.2017.03.011>
- Nkomo, V. T., Gardin, J. M., Skelton, T. N., Gottdiener, J. S., Scott, C. G., & Enriquez-Sarano, M. (2006). Burden of valvular heart diseases: A population-based study. *The Lancet*, 368(9540), 1005–1011. [https://doi.org/10.1016/S0140-6736\(06\)69208-8](https://doi.org/10.1016/S0140-6736(06)69208-8)
- Paeme, S., Moorhead, K., Chase, J. G., Hann, C. E., Lambermont, B., Kolh, P., Moonen, M., Lancellotti, P., Dauby, P. C., & Desai, T. (2010). *Mathematical model of the mitral valve and the cardiovascular system application for studying and monitoring valvular pathologies*. Control 2010, UKACC International conference On, C(L), 1–6. <https://doi.org/10.1049/ic.2010.0386>
- Pant, S., Corsini, C., Baker, C., Hsia, T. Y., Pennati, G., & Vignon-Clementel, I. E. (2017). Inverse problems in reduced order models of cardiovascular haemodynamics: Aspects of data assimilation and heart rate variability. *Journal of the Royal Society Interface*, <https://doi.org/10.1098/rsif.2016.0513>
- Razafindrazaka, F. H., Vellguth, K., Degener, F., Suendermann, S., & Kühne, T. (2019). *Mesh based approximation of the left ventricle using a controlled shrinkwrap algorithm*. Lecture Notes in Computer Science (including subseries Lecture Notes in Artificial Intelligence and Lecture Notes in bioinformatics): Vol. 11504 LNCS issue Lv, (pp. 230–239). https://doi.org/10.1007/978-3-030-21949-9_25
- Rosenson, R. S., McCormick, A., & Uretz, E. F. (1996). Distribution of blood viscosity values and biochemical correlates in healthy adults. *Clinical Chemistry*, 42(8), <https://doi.org/10.1093/clinchem/42.8.1189>
- Schwammenthal, E., Chen, C., Benning, F., Block, M., Breithardt, G., & Levine, R. A. (1994). Dynamics of mitral regurgitant flow and orifice area. Physiologic application of the proximal flow convergence method: Clinical data and experimental testing. *Circulation*, 90(1), 307–322. <https://doi.org/10.1161/01.CIR.90.1.307>

- Shi, Y., Lawford, P., & Hose, R. (2011). Review of zero-D and 1-D models of blood flow in the Cardiovascular system. *BioMedical Engineering OnLine*, 10(1), 33. <https://doi.org/10.1186/1475-925X-10-33>
- Sotaquirá, M., Pepi, M., Tamborini, G., & Caiani, E. G. (2017). Anatomical regurgitant orifice detection and Quantification from 3-D echocardiographic images. *Ultrasound in Medicine & Biology*, 43(5), 1048–1057. <https://doi.org/10.1016/j.ultrasmedbio.2016.12.017>
- Sun, H. T., Sze, K. Y., Tang, A. Y. S., Tsang, A. C. O., Yu, A. C. H., & Chow, K. W. (2019). Effects of aspect ratio, wall thickness and hypertension in the patient-specific computational modeling of cerebral aneurysms using fluid-structure interaction analysis. *Engineering Applications of Computational Fluid Mechanics*, 13(1), 229–244. <https://doi.org/10.1080/19942060.2019.1572540>
- Thavendiranathan, P., Liu, S., Datta, S., Rajagopalan, S., Ryan, T., Igo, S. R., Jackson, M. S., Little, S. H., De Michelis, N., & Vannan, M. A. (2013). Quantification of chronic functional mitral regurgitation by automated 3-dimensional peak and integrated proximal isovelocity surface area and stroke volume techniques using real-time 3-dimensional volume color Doppler echocardiography: In vitro and clinical. *Circulation: Cardiovascular Imaging*, 6(1), 125–133. <https://doi.org/10.1161/CIRCIMAGING.112.980383>
- This, A., Morales, H. G., Bonnefous, O., Fernández, M. A., & Gerbeau, J.-F. (2020). A pipeline for image based intracardiac CFD modeling and application to the evaluation of the PISA method. *Computer Methods in Applied Mechanics and Engineering*, 358, 112627. <https://doi.org/10.1016/j.cma.2019.112627>
- Vellguth, K., Brüning, J., Goubergrits, L., Tautz, L., Hennemuth, A., Kertzsch, U., Degener, F., Kelm, M., Sündermann, S., & Kuehne, T. (2018). Development of a modeling pipeline for the prediction of hemodynamic outcome after virtual mitral valve repair using image-based CFD. *International Journal of Computer Assisted Radiology and Surgery*, 13(11), 1795–1805. <https://doi.org/10.1007/s11548-018-1821-8>
- Vellguth, K., Brüning, J., Tautz, L., Degener, F., Wamala, I., Sündermann, S., Kertzsch, U., Kuehne, T., Hennemuth, A., Falk, V., & Goubergrits, L. (2019). User-dependent variability in mitral valve segmentation and its impact on CFD-computed hemodynamic parameters. *International Journal of Computer Assisted Radiology and Surgery*, 14(10), 1687–1696. <https://doi.org/10.1007/s11548-019-02012-1>
- Votta, E., Le, T. B., Stevanella, M., Fusini, L., Caiani, E. G., Redaelli, A., & Sotiropoulos, F. (2013). Toward patient-specific simulations of cardiac valves: State-of-the-art and future directions. *Journal of Biomechanics*, 46(2), 217–228. <https://doi.org/10.1016/j.jbiomech.2012.10.026>
- Weber, F. M., Stehle, T., Waechter-Stehle, I., Götz, M., Peters, J., Mollus, S., Balzer, J., Kelm, M., & Weese, J. (2015). Analysis of mitral valve motion in 4D transesophageal echocardiography for transcatheter aortic valve implantation. In O. Camara, T. Mansi, M. Pop, K. Rhode, M. Sermesant, & A. Young (Eds.), *Statistical Atlases and Computational Models of the Heart - Imaging and Modelling Challenges. STACOM 2014. Lecture Notes in Computer Science* (Vol. 8896, pp. 168–176). Springer.
- Yosefy, C., Hung, J., Chua, S., Vaturi, M., Ton-Nu, T. T., Handschumacher, M. D., & Levine, R. A. (2009). Direct measurement of Vena Contracta area by real-time 3-dimensional echocardiography for assessing severity of mitral regurgitation. *American Journal of Cardiology*, 104(7), 978–983. <https://doi.org/10.1016/j.amjcard.2009.05.043>
- Zoghbi, W. A., Adams, D., Bonow, R. O., Enriquez-Sarano, M., Foster, E., Grayburn, P. A., Hahn, R. T., Han, Y., Hung, J., Lang, R. M., Little, S. H., Shah, D. J., Sherman, S., Thavendiranathan, P., Thomas, J. D., & Weissman, N. J. (2017). Recommendations for noninvasive evaluation of native valvular regurgitation. *Journal of the American Society of Echocardiography*, 30(4), 303–371. <https://doi.org/10.1016/j.echo.2017.01.007>